HELSINGIN YLIOPISTO
HELSINGFORS UNIVERSITET
UNIVERSITY OF HELSINKI

MATEMAATTIS-LUONNONTIETEELLINEN TIEDEKUNTA
MATEMATISK-NATURVETENSKAPLIGA FAKULTETEN
FACULTY OF SCIENCE

Tiedekunta – Fakultet – Faculty	Koulutusohjelma – Utbildningsprogram – Degree programme
Matemaattisluonnontieteellinen tiedekunta	Fysiikka

Tekijä – Författare – Author

Aleksi Zitting

Työn nimi – Arbetets titel – Title

Irradiation effects in tungsten under fusion-reactor-relevant conditions

Työn laji – Arbetets art – Level	Aika – Datum – Month and year	Sivumäärä – Sidoantal – Number of pages
Pro gradu tutkielma	14.2.2019	45

Tiivistelmä – Referat – Abstract

Due to increasing energy demand and environmental concerns, developing cleaner and more efficient methods of energy production is becoming more and more important. One such method proposed is a fusion reactor. The plasma facing materials of the reactor must be able to withstand the harsh conditions inside. One such material proposed to be used in constructing the plasma facing components in the reactor is tungsten. In this work I examine the the durability of tungsten under fusion-grade conditions using molecular dynamics simulations.

First the impact of neutron irradiation of simulated by simulating 150 keV tungsten irradiation of a 65nm thick tungsten thin film. This was done at 800K and 1900K. After simulating the irradiation event, damage was determined by calculating Wigner-Seitz defects. Larger defect clusters where then analyzed to determine their type. For interstitial type defect clusters loops with the Burger's vector <100> and ½<111> formed with ½<111> loops being 4 times as common. For vacancy-type clusters craters, spherical voids and <100> loops formed, however no ½<111> loops formed even though they are seen in experiments. Temperature didn't seem to have an effect on the amount of defects formed, however the defects that formed were larger at 1900K than at 800K.

Secondly the co-bombardment of a tungsten surface with deuterium and a noble gas impurity was simulated. This process was done by randomly selecting either a deuterium ion or a noble gas ion, placing it above the surface and giving it a kinetic energy towards the surface. Several different cases were studied where the following variables were varied: noble gas species (neon or argon), impact energy (10,30,50,80,100 eV), noble gas concentration (5,10,20%) and temperature (500, 800 K). Damage was the determined by looking at the deuterium retention and reflection of the surface, the sputtered tungsten and change of surface morphology. Argon caused more damage than neon. Increasing irradiation energy increased the damage done to the surface, with tungsten sputtering being possible at 80 eV and above. Increased gas concentration also increased the damage. Temperature differences were only significant for deuterium reflection at low energies.

Avainsanat – Nyckelord – Keywords

Fusion Material physics Tungsten Molecular dynamics

Säilytyspaikka – Förvaringställe – Where deposited

Muita tietoja – Övriga uppgifter – Additional information

Master's thesis

Physics

Irradiation effects in tungsten under fusion-reactor-relevant conditions

Aleksi Zitting

2019

Advisors: Andrea Sand
Elnaz Safi
Examiners: Kai Nordlund
Andrea Sand

UNIVERSITY OF HELSINKI
DEPARTMENT OF PHYSICS

PL 64 (Gustaf Hällströmin katu 2)
00014 University of Helsinki

Contents

1 Introduction

Modern society is experiencing increased energy demand, climate change and environmental concerns. This means that development of cleaner and more efficient means of producing electricity is becoming more and more important.

One such proposed method for energy production is the harnessing of the energy released when light nuclei fuse together. Currently a promising option is the tokamak where a hot plasma undergoing a fusion reaction is contained in a toroidal magnetic field. The fusion reaction inside stellar cores such as inside the Sun is well understood and requires only regular hydrogen. However, these conditions are not possible on Earth and alternative means of fusion must be pursued. The most promising reaction and the one examined in this work is the fusion between the heavier isotopes of hydrogen; deuterium and tritium. Since we lack the pressure of the gravitational furnace that occurs at stellar cores, the method to make fusion feasible on Earth is increasing the temperature. This poses several challenges when it comes to building and maintaining a tokamak reactor. Additionally the fusion reaction produces energetic neutrons, which will escape the plasma, impacting in the materials of the reactor components, causing radiation damage.

In order for tokamak fusion reactors to be feasible for energy production, they must remain operational for decades. Thus the materials used in the reactor must remain functional for extended periods of time in order for operation to be possible. This means that it is important to study the damage that the reactor components suffer while the reactor is in operation. Therefore studying the damage formation mechanisms can lead to better, safer and cheaper energy production. [1]

Tungsten has been chosen as a suitable candidate to be one of the main materials to be used inside tokamak fusion reactor ITER and its successor DEMO for plasma-facing components (PFCs), due to its high sputtering threshold, low fuel retention and high melting point. However, tungsten is also brittle and irradiation causes radiation damage which over a longer timescale may lead to embrittlement, swelling or induced radioactivity resulting from the nuclear reactions due to neu-

tron radiation. This makes it an important material to study. [2]

In this work we will examine molecular dynamics (MD) simulation of damage formation in tungsten, since the timescales available to simulations allow us to look at how damage formation starts, which is currently infeasible experimentally both due to measuring such short timescales being practically impossible and because current test reactors do not properly replicate the conditions inside ITER or DEMO. Understanding how damage forms and evolves over time allows us to find ways to mitigate it and build more durable reactors allowing for more feasible energy production. However, MD simulations are not entirely accurate to what happens in the real world due to the numerous approximations and non-physical numerical optimizations required to simulate large enough atom arrays for a long enough period of time, meaning that attention must be paid to ensure that the results provided are realistic.

This work examines two different damage formation situations; irradiation of a tungsten thin film by tungsten ions, and deuterium-noble gas co-irradiation of a tungsten surface. Both cases are very relevant when it comes to operating a tokamak. Irradiating tungsten using tungsten ions provides similar conditions to the situation where high energy neutrons will escape the plasma. Due to not being charged particles, they can't be contained by a magnetic field. The neutrons will then damage the tungsten PFCs. This happens when they penetrate the surface and collide with a tungsten atom in the bulk. By giving a tungsten ion an energy similar to what it would receive in a collision with a neutron, the damage formation can be experimentally simulated. Deuterium-noble gas irradiation is relevant in keeping the plasma inside the reactor stable with occasional cooling. One such way is by injecting small amounts of noble gases in it. When these gases ionize, the plasma loses energy and becomes easier to contain. Even though the nuclei are charged, they will still leak from the plasma, especially at the bottom of the tokamak. They then deposit themselves on the PFCs. Due to being heavier and larger than typical plasma components, the damage they cause is potentially different.

2 Fusion in Tokamak-like reactors

In a fusion reaction two or more nuclei fuse together to produce a larger nucleus. If the resulting large nucleus has less binding energy per atom than that of the reacting nuclei, this reaction releases energy. In a reactor this energy is harnessed when the rector is heated. This heat is then transferred to water and used in a steam turbine to produce electricity.

For a fusion reaction to be considered worthwhile to produce energy it must fulfill several criteria. First, it must release energy, which means that only light nuclei that are less tightly bound can be used. This is due to light nuclei having less repulsion between them because of overlapping electron clouds, leading to more probable reactions. Secondly, reactions should have two reactants since three body collisions are much less probable than two body collisions. Thirdly, the nuclear cross section of the reaction, which determines the likelyhood of the reaction, should be large. For practical use one must also consider how easy the fuel for the reaction is to acquire and whether the reaction causes neutron radiation or not.

Currently one of the most efficient reactions and the current candidate for tokamak reactors is the fusion of deuterium and tritium which produces helium and a neutron. [3]

$$ {}^{2}_{1}D + {}^{3}_{1}T = {}^{4}_{2}He\ (3.5\ \text{MeV}) + n^{0}\ (14.1\ \text{MeV}) \tag{1} $$

This is due to the large reaction cross section, large amount of energy produced per nucleus and the relative ease of acquiring the fuel. Deuterium can be extracted from sea water. Tritium is rare in nature but can be produced by a neutron-lithium reaction [4]

$$ {}^{6}_{3}Li + n^{0} = {}^{4}_{2}He + {}^{3}_{1}T + 4.8\text{MeV} \tag{2} $$

or

$$ {}^{7}_{3}Li + n^{0} = {}^{4}_{2}He + {}^{3}_{1}T + n^{0} - 2.47\text{MeV} \tag{3} $$

which happens when the neutron produced by the D-T reaction hits a lithium

blanket inside the reactor. This process is called tritium breeding and is the main source of tritium in a Tokamak. [5]

The two nuclei have to get really close to each other for the strong interaction to dominate over the repulsive electromagnetic potential. A star solves this problem with extremely high gravitational pressure greatly increasing the probability of a reaction. Since the density of a stellar core is not possible on Earth this problem is solved instead by using extremely high temperatures. The temperature causes the fusion reactants to fully ionize, turning into a plasma which is a globally neutral gas consisting of charged particles; ions and electrons.

The temperature required for a fusion reaction to sustain itself is extremely high, around $10^8 K$ [6]. This means that the plasma must be contained in a vacuum since no known solid material could withstand these temperatures. The confinement is done via a magnetic field since the plasma consists entirely of charged particles. In a tokamak the magnetic field contains the plasma in a toroidal shape, which means that there are no end losses, since there are no ends on a torus. The toroidal confinement is done by having several coils form a toroidal field. [7]

Since the coils are closer together at the center than at the edge, the field strength is proportional to $\frac{1}{r}$, where r is the radius of the torus. This will cause the charged particles to drift radially, with ions and electrons drifting in opposite directions. This charge separation causes an additional electric field which then causes both particles to drift radially away from the plasma. In a tokamak this problem is solved by inducing a current in the toroidal direction. This current is induced by a central transformer. Additionally the plasma will expand radially when it heats, which means that vertical coils are needed to restrain that expansion. To increase the efficiency of the magnets, they are kept superconducting by cooling them down to very low temperatures. The shape of these magnets determines the shape of the cross-section of plasma which determines how stable and efficient the fusion is. The first tokamaks had a circular cross section, but modern designs often have a D or C-shaped cross section. The D-ring variant of the coils and magnetics fields is shown in Figure 1. [7]

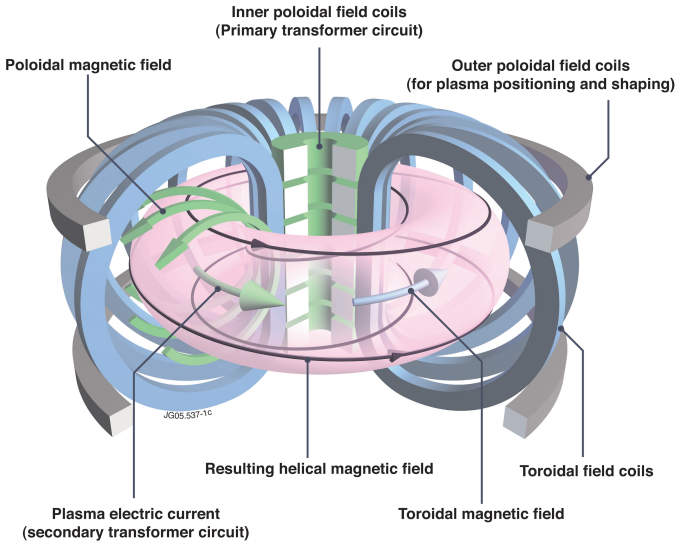

Figure 1: Coil setup for a tokamak reactor. [8]

The operating temperature of the plasma is over 10^8 K which means that the plasma must be heated up to this point at the start-up. Initial heating can be done by simple Ohmic heating. Since a current has to be induced into the plasma to provide the necessary poloidal field, this same current produces heat. By increasing the induced current the plasma can be heated up. Since increasing the temperature of the plasma decreases the resistance of the plasma, increasing the current only provides enough energy to get the plasma to the range of 10^7 K. [6]

Further heating is usually done by neutral beam injection (NBE). First, some material is ionized by microwaves or other means. These ions are then accelerated in an electric field, and after that neutralized by adding back the opposite charge. These fast moving neutral particles are then injected into the plasma, heating it up when they collide with plasma particles. The reason the injected particles have to be neutral is that charged particles might not penetrate the confining magnetic field clearly and cause instabilities. Often fusion reactants such as hydrogen or deuterium are used in the NBE since they will be used as fuel afterwards. [6]

In a D+T fusion reaction most of the energy is deposited to the neutron which doesn't remain in the plasma due to having no electrical charge. However, the

roughly 3.4 MeV that the He-4 ion (α-particle) receives remains in the plasma, heating it up. At sufficient temperatures, this reaction happens often enough that the energy created both by the reaction itself and harnessed from generators for ohmic heating is enough to offset the energy losses due to bremsstrahlung, impurity radiation at the edges, charge exchange and hydrogen radiation. [9]

While less energy efficient, the reaction will be more stable at lower temperatures [10]. Therefore it's important to sometimes cool down the plasma in order to increase the stability of the plasma. One way to do this is by injecting small amounts of noble gases into the plasma. When these inert gases ionize, they absorb energy from the plasma, decreasing its temperature.

Despite all this, the plasma is still not confined perfectly and particles will escape the plasma. Additionally, the neutrons produced do not interact with the magnetic and electric fields, and will escape the plasma. This means that high energy particles escaping the plasma will interact with materials inside the fusion reactor, possibly damaging them. In order to have a feasible reactor design, the plasma facing components (PFCs) must be able to handle heat and particles commonly used and produced in the plasma.

PFCs should have a high melting point and a low vapor pressure. They should also be able to handle neutron radiation by having a low neutron activation, since a neutron can make materials radioactive through neutron activation. Low tritium retention is desirable to prevent a loss of significant amounts tritium which is needed to fuel the reaction. Low thermal expansion and high heat conductivity are needed to keep the structure intact and easy to cool. The material will regardless be eroded by high energy particles, causing it to end up in the plasma. This makes materials with low atomic numbers preferred since the plasma is cooled down less due to a lower ionization energy. Being chemically inert is also desirable. Additionally the price and availability of the materials must be considered when trying to design a viable reactor. [11]

For ITER there are several materials to be used in different PFCs. The fusion reaction is contained in a vacuum vessel which is mostly made from steel. The

vacuum vessel is covered with large blanket modules which shield the vessel from heat and radiation. These blankets are made from steel and copper. The blanket module is covered by a wall called the first or main wall. Beryllium is the current material of choice for the main wall due to plasma having a high tolerance for Be impurities due to its small electron number (Z=4), and Be having desirable thermal and mechanical properties despite its toxicity. Some modules may also contain lithium which is needed for tritium breeding. [12]

The divertor is a component located at the bottom of the tokamak which gets rid of impurities in the plasma by guiding them out using magnetic fields. D-T fusion creates He-4 ions which are commonly referred to as "helium ash" in the context of fusion reactors. This "ash" dilutes the plasma, causing reactions to happen less frequently. Divertor guides helium ash and other impurities due to sputtering of surface materials out of the plasma. Due to this the divertor has to handle both higher than normal particle fluxes and temperatures higher than the other PFCs. The current divertor of ITER is shown in Figure 2. [13]

Tungsten is the current choice for the plasma facing material in the divertor [14]. Tungsten was chosen because it has the highest melting point of all metals, low vapor pressure, low neutron activation, good thermal properties and has a low tritium retention. However tungsten is also very brittle, and due to its high Z, the plasma has a low tolerance for tungsten impurities. If air leaks into the reactor, tungsten can also oxidize. Tungsten is also in consideration for the main wall material in DEMO.

Figure 2: Picture of the divertor [15]

Ultimately a tokamak and all other fusion reactor types must be able to turn the thermal energy from the reaction into electricity. This is accomplished in the same manner as most other reactor types based on a chemical or nuclear reaction. The heat from the reaction is used to boil water, which then runs a steam turbine which drives an electric generator.

3 Ion and neutron radiation effects in metals

3.1 Mechanisms of damage production

Irradiation can damage materials by changing its structure from the usual, such as a perfect crystalline structure, into something else. This happens at microscale when the particles from the radiation source interact with the atoms in the material by depositing energy into them. Most solid materials have some sort of structure, such as having the atoms form a lattice for crystalline materials like metals. Deviance from the regular structure is considered damage.

For crystalline materials, if an atom is knocked out of its lattice point by irradiation, it forms a defect called a Frenkel pair. The Frenkel pair consists of a *vacancy* (lattice point with a missing atom) and an *interstitial* (an atom outside of a lattice point). These defects also form spontaneously under finite temperatures with increasing rate of formation at higher temperatures. The point defects can move around at finite temperatures, and once they reach a surface or when an interstitial combines with a vacancy the defects disappear. Ion irradiation may also cause the introduction of impurities into the material, which might substitute other atoms or change the structural configuration due to the difference in size or electronic properties of the ion compared to the target material. [16]

The point defects can form clusters with each other, leading to formation of higher dimensional defects in the material. These defect clusters can also move around and combine with other defect clusters, leading to defect evolution. The formation of these microscopic defects and their evolution may eventually lead to macroscopic

changes in the properties of the material. For example: vacancies clustering to form voids which leads to the material becoming porous in the macroscale and thus being less stress resistant.

When a particle enters a target material and collides elastically with atoms in the target, if the recoil energy exceeds the threshold displacement energy (TDE) of the material, the atom will be displaced from its lattice site. This displaced atom is called a primary knock-on atom (PKA). If these PKAs have enough energy, they can collide with further atoms, where the elastic collision also exceeds the TDE, producing secondary knock-on atoms which can then produce tertiary knock-on atoms and so on. For a simplified illustration, see Figure 3. Since the collisions will rarely transfer all the energy from one atom to the next, subsequent generations will have less kinetic energy than the previous one and eventually their energy is not sufficient for damage production. At very high energies, the secondary knock-on atoms have such high energies that they may travel deep into the material away from the original cascade, causing distinct subcascades. [16]

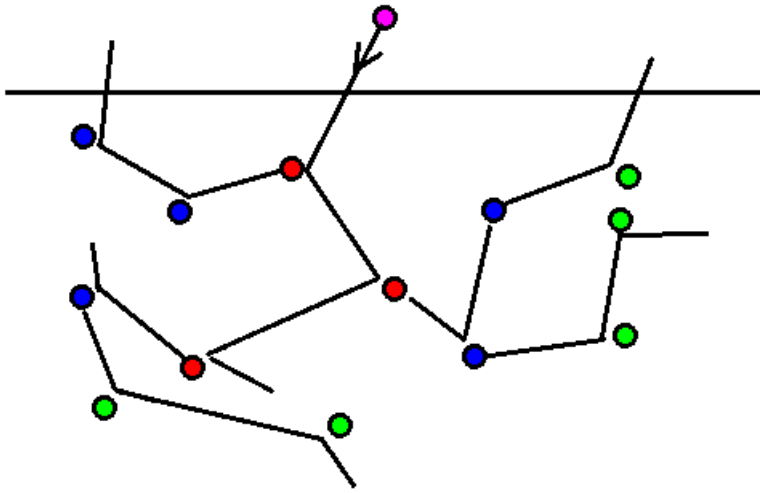

Figure 3: Simplified illustration of a cascade. Incoming ion (magenta) hits the target surface and collides with red atoms (primary knock-ons), which collide with blue atoms (secondary knock-ons), which then collide with green atoms (tertiary knock-ons).

When a material is irradiated with ions at lower energies, most of the interaction between the ions and the material comes from nuclear stopping, where the ions collide elastically with the atoms of the target material. This gives kinetic energy to the atoms in the material while the ion loses energy.

At higher irradiation energies, a significant part of the interaction with the material is caused by electronic stopping, which is caused by the ion interacting with the electronic clouds of the surrounding atoms. This causes the electronic states of the ion and the surrounding atoms to change. This means that this process is inelastic, since a part of kinetic energy is transferred to excitations. At even higher energies (hundreds of MeV) electronic stopping becomes negligible compared to stopping due to bremsstrahlung from rapid deceleration near the speed of light, Cherenkov radiation from having a faster phase velocity than speed of light in that material, and nuclear reactions from colliding nuclei. A simulation showing the relation between nuclear and electronic stopping is shown in Figure 4.

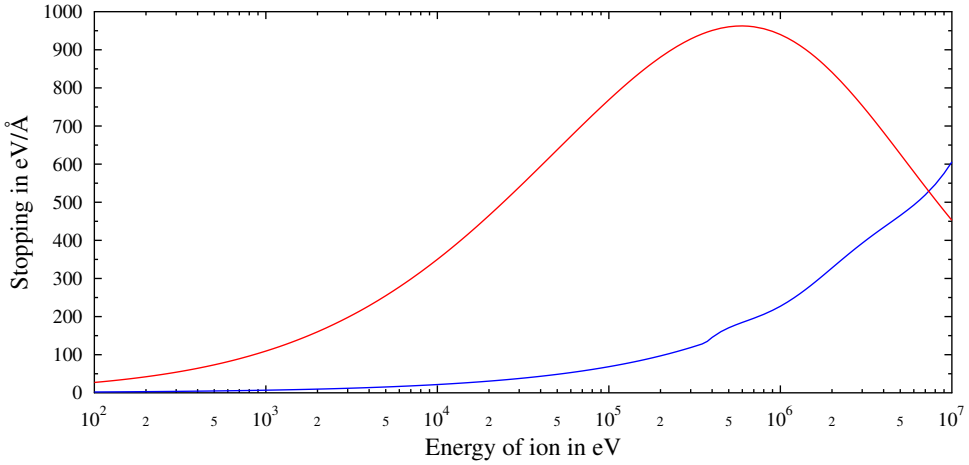

Figure 4: SRIM [17] simulation of stopping power of tungsten ions in tungsten. Red represents nuclear stopping and blue represents electronic stopping. Electronic stopping starts becoming significant compared to nuclear stopping in the 10 keV range.

A fast moving ion or a knock-on atom will deposit a part of its energy to a small area due to electronic stopping which then quickly dissipates through heat diffusion. This causes a heat spike in the area the ion passes through. There the temperature quickly rises to large values and then quickly cools down. This heat spike lasts long enough for the kinetic energy of the atoms to follow a Maxwell distribution. When the system cools down, the disordered atoms in the heat spike go mostly back to their original crystal structure. But due to the quick cooling, some defects don't have time to settle into the optimal lattice structure, which means that defects will form during the cooling.

Since the time scale of heat spike formation and cooling is so small, the experimental study of them is extremely difficult, or impossible, with current methods. In order to study damage formation in a heat spike, computational simulations are used instead. Solving the Schrödinger equation individually would provide an extremely accurate description (assuming all parameters are known), but in the simulated systems there are too many atoms and the time scale is too long for this to be feasible.

Simulating a collision cascade by tracking individual atoms is done either with binary collision approximation (BCA) or by molecular dynamics (MD) simulations. BCA is a very efficient method where the fast moving ion moves through the matter and experiences elastic binary collisions with target atoms. Between collisions, it loses energy only to electronic stopping. MD simulations also take into account the interactions between the ion and nearby atoms that the target atom doesn't collide with. This leads to more accurate but slower to calculate results. Due to increased computing power and need for accuracy, MD is typically used over BCA for damage formation simulations.

3.2 Radiation effects in fusion reactors

Due to the high temperatures and nuclear reactions inside a fusion reactor, there are many different types of radiation that need to be taken into account when

designing a fusion reactor where the damage caused by the radiation does not affect the operation of the reactor over its lifetime.

The plasma contains D,T,He, impurities and possibly noble gas ions if needed for cooling the plasma. The plasma isn't perfectly contained and these ions in it will end up outside of it, especially near the divertor. This means that materials will be exposed to low energy (≤ 1 keV) ion irradiation. Materials will therefore interact with the plasma, which causes sputtering and retention of ions in the material. Chemical processes are also possible due to the ions coming into contact with surface materials.

The standard D + T fusion reaction produces energetic 14.1 MeV neutrons which are not contained by the magnetic fields. This means that all plasma facing components will have to endure neutron radiation. While these high energy neutrons cause displacement of atoms leading to defect formation, they also may induce nuclear reactions in the PFCs causing the atoms to transform into impurities. Additionally, these impurities may be radioactive isotopes, leading to PFCs becoming activated. In tungsten, the material chosen for this work, neutron irradiation mainly results in osmium and rhenium isotopes [18]. However the long term effects such as increased radioactivity and introduction of new impurities through nuclear reactions are beyond the scope of this work.

Neutron radiation is of much higher energy than ion radiation. This means that neutron radiation inside a fusion reactor mostly affects the bulk while ionic radiation is generally near the surface. Due to the difference in the irradiation energy, flux and the affected area, particle size, the damage production differs greatly with different forms of radiation.

Experimental testing of neutron irradiation is difficult due the difficulty of producing high energy neutrons and because the samples will suffer from neutron activation. And since neutrons tend to penetrate deep into materialsm imaging the damaged materials is difficult. Neutron radiation can however be mimicked by ion irradiation. When a high energy neutron hits an atom, it gives it some amount of energy depending on the recoil spectrum. Thus, on average the neutron will

give the atoms a certain amount of energy, for example the average energy a 14.4 MeV neutron gives to a tungsten atom in a collision in 150 keV. Similar damage can be produced by irradiating the target material with ions of that material with a specific energy. However, because they are ions this radiation doesn't penetrate as deep as neutron radiation and is thus susceptible to surface effects. However, it's easier to image surfaces and thin films than bulk which makes damage easier to visualize.

Recent work has been done to irradiate tungsten thinfilms using 150 keV W ions. These films can be imaged in their entirety by using transmission electron microscopy to find how defect structures evolve during irradiation. [1]

4 Molecular dynamics

4.1 Basics of molecular dynamics

Molecular dynamics is a numerical method for solving a classical N body problem consisting of atoms and/or molecules. A molecular dynamics algorithm first reads in the positions of the atoms and a function that defines the potentials and forces between them as a function of distance. Then by integrating Newton's equations of motion over a small timestep Δt, the positions of the atoms are updated. In practice this is done by using for example Verlet integration

$$x_{n+1} = 2x_n - x_{n-1} + \frac{F}{m}(\Delta t)^2, \tag{4}$$

where the position of an atom at the next step depends on its position during the last two steps and the force acting on it. [19]

This algorithm depends on the timestep chosen. With large time steps, the positions are not updated frequently enough and the atoms may end up in positions which would cause the system energy to increase leading to unphysical results. However if the timestep is too small, the amount of time a computer would spend on the simulation would be infeasibly large. Thus the timestep must be chosen

carefully so that it provides accurate results while not being too cumbersome to run.

If the system simulated is not very small, it's usually neither necessary nor practical to consider the interaction of every particle with every other particle since this would increase the time required for very little benefit, especially since calculating forces is one of the most time consuming parts of MD simulations. Thus, when calculating the force experienced by a particle, only its close neighbors are considered. This is usually done simply by ignoring all particles outside some predefined radius r_{cut}. However, updating this list of neighbors during every timestep is also inefficient, which would be necessary due particles movement. Instead every particle has a neighbor list which contains all neighbors inside r_{cut} and particles outside r_{cut} which could potentially be neighbors within the update frequency of the neighbor list. [19]

A standard MD simulation happens in a microcanonical ensemble (NVE) where the particle number, volume and energy of the system are all constant. This may be accurate for very small systems but in most real world applications the system is much larger than those possible to calculate purely using MD in an NVE ensemble. Usually the simulated system is considered to be a small part of a larger system which it is loosely connected to [19]. This means that when introducing energy to a small part it will dissipate quickly in the form of heat. Thus usually the systems are simulated as a canonical ensemble (NVT) where the temperature is kept constant by some thermostat or as a isothermal-isobaric ensemble (NPT), where in addition to constant temperature, the pressure is also kept constant by some barostat. These more accurately reflect real life conditions in most cases.

One other way to approximate a large system with just a small part of the total system is with periodic boundary conditions. Periodic boundary conditions can be used if the system size is so large that it can on average be considered to be similar to bulk and that the artefacts caused by the boundary conditions with energy or particles travelling from one boundary to another are minimal. Periodic boundary conditions can be applied to as many directions as desired, to simulate different

systems. If x,y and z directions all have periodic boundaries, the system is similar to bulk. If x and y are periodic, the system is a film or a "slab". If only x is periodic, the system is a long rod or a wire.

When simulating the surface of a bulk material, it's necessary to have the boundary open in only one direction. This is done by fixing the atoms at the bottom by fixing their positions and attaching a thermostat to next layers of atoms, which makes the atoms at the bottom behave as if attached to bulk, while the atoms at the top act as a surface. See Figure 5 for an example.

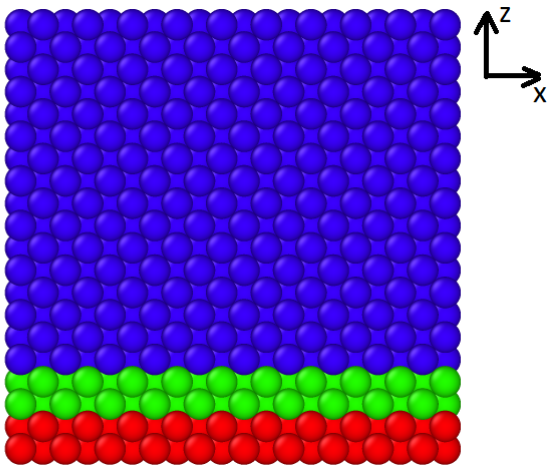

Figure 5: Example setup of surface simulation. Red = atoms with fixed position, green = atoms with fixed temperature, blue = free atoms.

An MD simulation is essentially numerical solving of multiple differential equations. One such way is the predictor-corrector method. In this method, an initial guess value is calculated during the "predictor stage" using the initial values. This guess value is then modified by calculating a new corrected value using the values after a timestep Δt during the "corrector stage". A flowchart showing a predictor-corrector MD algorithm is shown in Figure 6. [19]

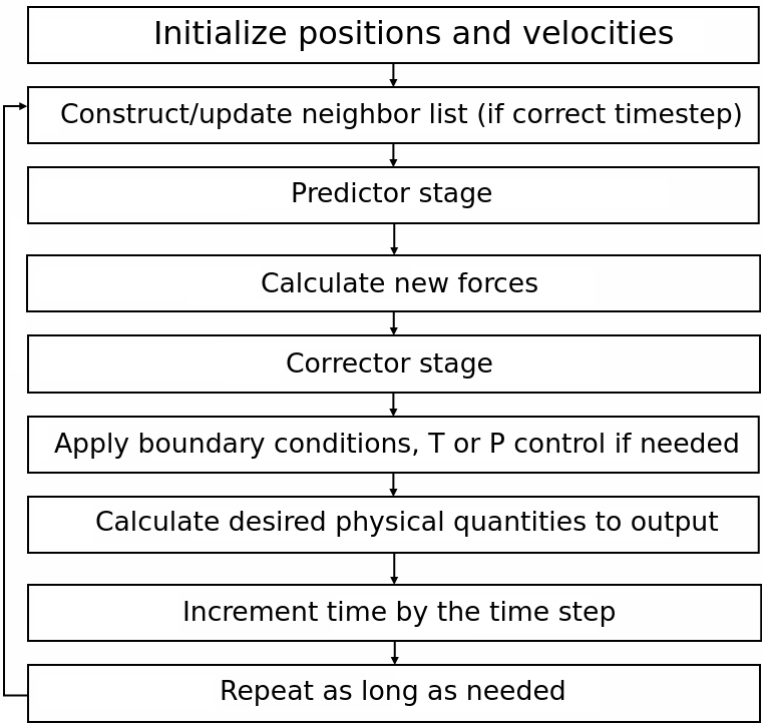

Figure 6: Simple algorithm for a predictor-corrector molecular dynamics simulation.

In molecular dynamics the forces acting on particles are determined by classical interatomic potentials. In regular MD, the Born-Oppenheimer approximation [20] holds. This means that the electrons are assumed to move much faster than nuclei which means that electromagnetic field of an atom doesn't change when moving. There are multiple different kinds of interatomic potentials. The used potential should provide reasonable accuracy, be reasonably fast and correctly predict properties which weren't used to fit the potential to the material.

A simple potential used to described interaction between a pair of atoms is the Lennard-Jones potential [21], which takes the form

$$V(r) = 4\epsilon \left[\left(\frac{\sigma}{r}\right)^{12} - \left(\frac{\sigma}{r}\right)^{6} \right], \tag{5}$$

where r is the distance between two atoms, ϵ is the potential well depth and σ is the distance at which the potential is zero. The potential consists of two terms.

The r^{-12} term describes the Pauli repulsion due to overlapping electronic orbitals, while the r^{-6} term describes the attraction between atoms due to long distance van der Walls forces. A plot that shows the form of the Lennard-Jones potential is shown in Figure 7.

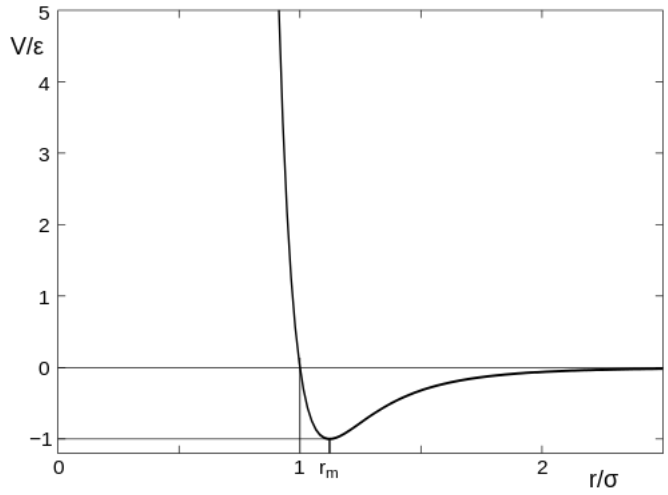

Figure 7: Graph of potential strength versus distance for Lennard-Jones potential. r_m is the distance at which the potential is at minimum.

Lennard-Jones and other pair potentials may be sufficient for simple cases such as simulating inert gases. However, they ignore the fact that the environment of an atom has a significant impact on the forces acting on it due to individual bond strength depending on how crowded the environment is. For example, there are far fewer other electrons at surfaces than in bulk. Pair potentials also do not care about individual bond direction, rotation or vibration. This is solved using many-body potentials, where in addition to the pair potential term, there are other many-body terms which describe the environment of the atom.

In metals the electronic environment of an atom is extremely important due to the nature of metallic bonding, where the outer electrons of the atoms are highly delocalized. A commonly used potential for metals is the EAM (Embedded Atom

Model) potential [22], where the potential energy of an atom i is

$$E_i = F_\alpha \left(\sum_{i \neq j} \rho_\beta(r_{ij}) \right) + \frac{1}{2} \sum_{i \neq j} \phi_{\alpha\beta}(r_{ij}). \tag{6}$$

This equation consists of the pair-wise core-core repulsion part $\phi_{\alpha\beta}$ and the embedding function part F_α, which represents the energy the atom gets when embedded in the electron clouds of nearby atoms represented by electron cloud density ρ_β. Thus in an EAM potential, every atom is considered an impurity that is embedded in the material. EAM potential is a multibody potential and thus more accurate than pure pair potentials such as Lennard-Jones. Due to its accuracy with metals and still being relatively fast, EAM is widely used in molecular dynamics.

4.2 Simulating irradiation effects with molecular dynamics

Simulating irradiation effects with molecular dynamics differs from standard MD simulations due to some atoms having a much higher kinetic energy than others. Generally in an irradiation event at the start there is a single atom with a much higher energy than the atoms in the irradiation target. However, as the simulation goes on this energy tends to dissipate in the material. Since there are a few fast moving atoms at the start and none at the end, a variable timestep is used to save resources and increase accuracy. A large timestep for the entire simulation would mean drastically inaccurate results and a small timestep would waste too much time at the end of the simulation when all atoms have roughly the same kinetic energy. [23]

In irradition simulations with a variable timestep, the timestep is inversely proportional to the highest velocity a particle has in the system. Additionally, if a particle experiences a strong force due to a collision, the timestep is made small because the velocity might be low at that moment, but the particle will soon accelerate to a high velocity. Otherwise the timestep will drift towards the default timestep it would have when the system is at equilibrium. Additionally if something leaves the system by for example sputtering, it will no longer be accounted

for when determining the next timestep. [23]

Another effect that comes into play at higher particle energies is electronic stopping. Accurate description of electronic stopping is very difficult due to the large amount of collisions with electrons the ion experiences while moving. The ion will also change its charge state multiple times. Electronic stopping and nuclear stopping are taken into account as stopping power

$$S(E) = -\frac{dE}{dx}, \tag{7}$$

which tells us how much energy an ion with a certain kinetic energy loses while travelling through a material, so it acts as a frictional term for the ion. Electronic stopping can be described theoretically by the Bethe-Bloch [24] formula which is relatively accurate for energies above 100 keV. However, at lower energies theoretical treatment of electronic stopping is difficult. [25]

Nuclear stopping is caused by elastic collisions between particles. These collisions are determined by the repulsive potential between two atoms. Thus extra care needs to be taken with the repulsive part of the interatomic potentials. In irradiation particles get close enough for the repulsion between two nuclei being the dominant force. Potentials which describe the repulsive part of the potential accurately must therefore be used. [25]

At very short distances the repulsion can be considered to be Coulumbic. At larger distances the electron clouds shield the nuclei from each other and the interaction becomes

$$-\frac{1}{4\pi\epsilon_0}\frac{Z_1 Z_2}{r^2}\phi(r) \tag{8}$$

where $\phi(r)$ is the screening function (1 at $r = 0$, otherwise < 1). Semi-empirical and theoretical methods are both used to find accurate repulsive potentials and screening functions. They can also be determined by using quantum mechanical numerical approaches such as density field theory. [26]

In case of neutron irradiation the neutron itself is not simulated. This is due to neutrons penetrating very deep into materials which would require infeasible

amounts of particles to be simulated. Instead neutron irradiation is simulated by giving an atom in the simulation cell kinetic energy equal to the average kinetic energy to represent an elastic collision with a neutron.

For ion irradiation, simulating the irradiation is done by placing a single ion somewhere near the target and given some specified velocity equivalent to the desired kinetic energy in some direction.

Continued bombardment can be simulated by repeating the simulation multiple times using the result of the previous simulation as the initial configuration. The reason why only the effects of a single ion at time need to be simulated is that even in generous and computationally demanding cases of large surfaces (>1000 nm^2) simulated over a large time (several ns), the particle flux while simulating irradiation is still several magnitudes above experimental and practical conditions. Though this does mean that simulation of effects with a fluency dependence may not be accurate.

5 Tungsten surface cascades

5.1 Setup and analysis

The simulations were performed using the molecular dynamics code PARCAS [27]. The simulated system was created by forming a BCC tungsten lattice which was rotated by approximately 14 degrees with respect to the xy-plane. The lattice size was 50 nm x 45 nm x 65 nm which resulted in a lattice a bit less than 9 million atoms large. The lattice constant when creating the lattice was chosen depending on the temperature according to the equation

$$a_0 + bT + cT^2, \tag{9}$$

where a_0 is the lattice constant at 0K while b and c are constants which depend on the material. Electronic stopping was implemented as a friction term using values gotten from a SRIM [17] simulation. Additionally an energy threshold of

$T_c = 10$ eV was applied, where electronic stopping was not applied to atoms below T_c because otherwise thermal effects are quenched too quickly. A time-lapse of an example simulation can be seen in Figure 15.

At 800K, the lattice was first relaxed with pressure control and periodic boundary conditions in all directions to eliminate pressure waves caused by relaxation. After this the system was relaxed without pressure control or periodicity in the z-direction. At 1900K, the same process was performed but first once at 1000K and then again at 1900K since relaxing only once at 1900K was not sufficient in eliminating pressure waves.

Eliminating pressure waves caused by the relaxation process was the largest problem with the simulation. Using pressure control in the actual cascade simulation was not possible, so they had to be gotten rid of almost entirely during relaxation. If this was not done, they created large amounts of defects unrelated to the cascade which made defect analysis practically impossible.

The cascade itself was simulated by randomly choosing an atom at the surface, near the center of the film, which was given a kinetic energy of 150 keV. The direction was also chosen randomly between 10 and 20 degrees with respect to the surface. If an atom with a kinetic energy of over 10 eV passed a periodic boundary (x and y directions), the simulation was killed to prevent unphysical results.

The system was simulated first for 60 ps. After that, an initial analysis was performed to determine if the relaxation needed to be continued. Another problem with the simulations seemed to be that in some cases the surface cooled very slowly despite additional relaxation time. Defects near the surface did not seem to stabilize, but remained mobile for long periods. Largest relaxation time tried was 200 ps did not seem long enough.

After the relaxation, if there were defect clusters larger than 10, the system was cooled down to 0K, to make defects and the atoms surrounding and especially their potential energy more visible compared to thermal fluctuations. After this the defect clusters were analysed using both numerical size and position analysis

and qualitative analysis to determine size and type of the defect.

The lattice defects created in the simulation were determined with Wigner-Seitz analysis. This is done by first determining the Wiger-Seitz cells of the initial lattice. A Wigner-Seitz cell is a volume centered on an atom which contains all points closer to the central atom than any other atom. [28] Additional defect analysis was performed by looking at atoms with a higher than average potential energy (roughly 0.1-0.2 eV higher than bulk, ignoring surfaces) which helped in identifying defects in addition to Wigner-Seitz analysis.

After creating the Wigner-Seitz cells and overlaying them on the final lattice one can find out the defect location and type. If the cell contains 1 atom, there is no defect. If the cell lacks an atom, it's a vacancy. If the cell contains 2 atoms or more, it's an interstitial. If the atom does not belong to a cell, it's either and adatom or a sputtered atom. This is determined by finding out if the atom connects to a surface through other adatoms or not.

After determining the defect locations, defect clustering was analysed. This was done by calculating if a defect is close enough to another defect of the same type. From this the sizes of the defect clusters were determined. After this atoms near the surfaces and atoms with low potential energy were filtered out to help with visualizing the defect clusters.

The visualisation was done using the program OVITO [29], which helped with determining the type of defect cluster in question. Special attention was paid to loops. By comparing the loop with how the energetic atoms near the cluster surrounded it, the Burgers vector could be determined. In unclear cases, the rest of the lattice was used to manually calculate the Burgers vector from the lattice.

5.2 Results

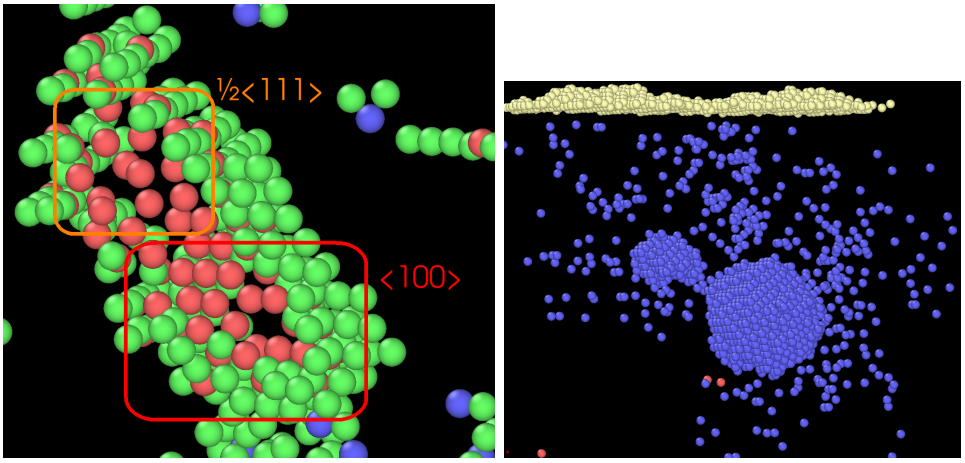

Figure 8: On the left a hybrid interstitial loop, consisting of both <100> and $\frac{1}{2}$<111> loops. Red indicates interstitials, blue vacancies and green atoms with a higher potential energy than bulk. On the right, two spherical voids.

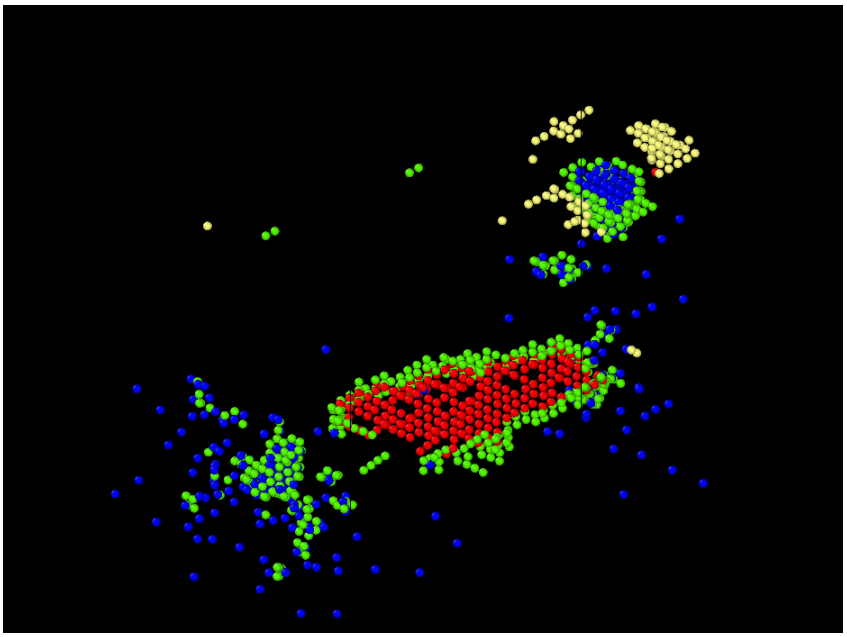

Figure 9: In the middle a <100> interstitial loop from above. Green indicates atoms with a high potential energy, blue vacancies and yellow adatoms.

Many different defect types formed during the simulation. The most common defects were single vacancies or SIAs, but larger structures were not uncommon. Special attention was given to defect loops, cconsisting of either interstitials or vacancies, due to their role in damage evolution.

SIA loops with Burgers vectors of both <100> and $\frac{1}{2}$<111> and vacancy loops with a Burgers vector of <100> were seen in the simulation.

Division into different Burgers vectors can be seen in Figure 8, where two different loops have fused into one. Due to the boundary between a defect and bulk, the defects are surrounded with atoms of higher potential energy. These high energy atoms tend to form a line with the $\frac{1}{2}$<111> defects and cluster around <100> defects. These vectors also tell how the loops can move in the tungsten lattice.

In addition to SIA loops, vacancy loops were also seen. But mostly at the higher temperature and much less often than SIA loops. They were also larger than SIA loops.

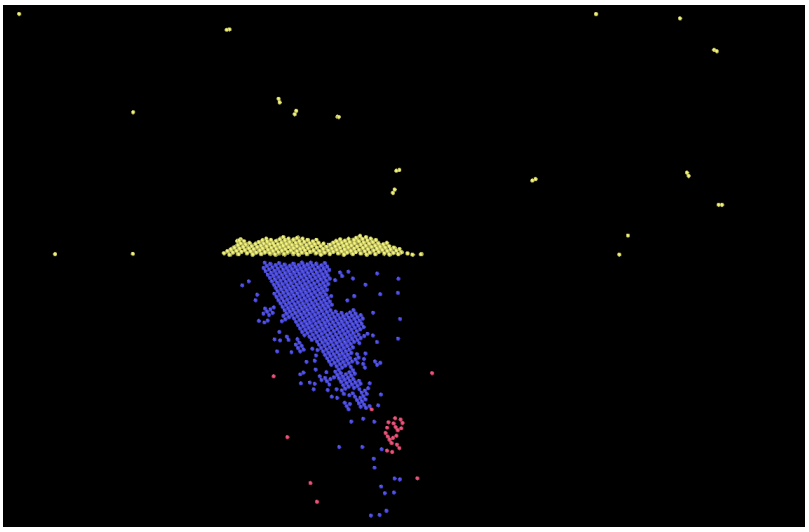

Figure 10: Crater (blue) caused by the cascade. Also pictured are adatoms (yellow cluster in the middle) and sputtered atoms (yellow atoms above the surface).

In addition to single defects and loops there were also spherical voids (Figure 9).

Often the cascade also formed craters with raised edges. Craters (Figure 10) were much more active than defects deeper in the film because the defects near them did not seem to relax nearly as fast. Additionally there were some smaller SIA and vacancy clusters which could not be categorized.

Average penetration depth of the recoil atom for the 800K case was 14.93 $\pm$ 1.67 nm while for the 1900K case it was 16.61 $\pm$ 2.22 nm. Additionally at 800K, there was a single case where the recoil atom penetrated through the whole film. Ignoring this case, the maximum penetration depths were 36.85 nm for 800K and 34.59 nm for 1900K.

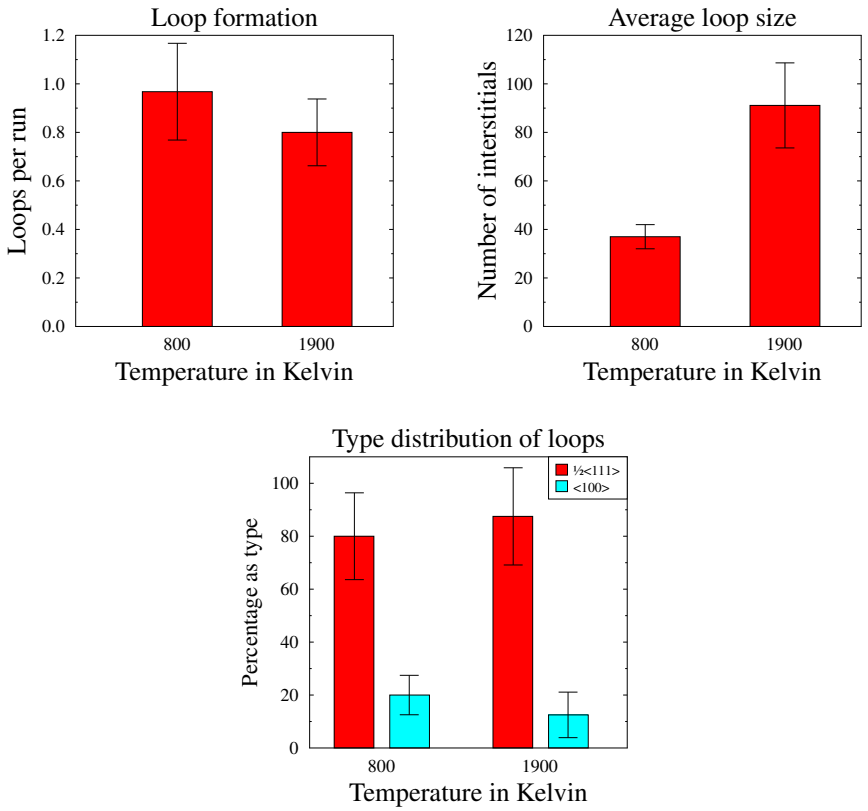

Figure 11: Properties of SIA loops with respect to temperature.

From Figure 11 we can see that loops are less common but larger at the higher temperature.

In 800K simulations 30 SIA loops were seen but only 1 vacancy loop. In 1900K simulations 17 SIA loops and 3 vacancy loops were seen.

Distribution of Burgers vectors can be seen from Figure 8, but vacancy loops were always $< 100 >$. Vacancy loops are seen in experiments [1], but are rare in simulations. According to experiments, at 800K $\frac{1}{2} < 111 >$ vacancy loops are as common as SIA loops of the same type but none were seen in the simulations. Experimentally 90% of $< 100 >$ loops were SIA loops at 800K. Some of the discrepancies can be explained with the fact that experimentally only loops larger than 1nm could be seen but only with loops larger than 4nm, was it possible to determine the type and Burgers vector of the loop. Simulations had very few large loops, so statistical analysis was not possible. The lack of $\frac{1}{2} < 111 >$ vacancy loops is still puzzling. [1]

The number of sputtered atoms was found to be much larger at 800K than at 1900K (Table 1). Cratering was observed for about 35% of the cases for 800K and only 20% of the cases for 1900K. This means that at the lower temperature, more damage formed at the surface, leading to increased sputtering. 800K cases also yielded no sputtering only 10% of the time while 1900K had no sputtering 40% of the time. Sputtered atoms were either as single W atoms or W^2 molecules. Additionally at 1900K there were several W^3 molecules which were very rare at 800K.

At 1900K more interstitials were created than at 800K (Table 1). At 800K more vacancies were created. Due to the damage analysis starting from a defect free lattice, the number of vacancies must be the same as the sum of interstitials, adatoms and sputtered atoms. They still differ slightly because an interstitial in the W-S analysis can contain multiple atoms.

The maximum of total vacancies (Table 1) for both cases wasn't very different despite the cause being a spherical void for 800K and a large vacancy loop for 1900K. At 1900K the minimum was larger than at 800K due to the fact that defects form on their own more often at higher temperatures. The minima for interstitials were not significantly different, but the maxima were. This is probably due to how

800K formed craters more often which kept interstitials from relaxing.

Looking at cluster size distributions (Figure 12) one can see that vacancies only form clusters 50% of the time, but interstitials over 75% of the time. How the defects belonged to different cluster sizes wasn't significantly different between the temperatures with vacancies except for slightly more vacancies clustering at small sizes (2-10) at lower temperatures. At 800K SIAs seemed to form small and midsized clusters while a very large portion of SIAs at 1900K were in large clusters.

For both SIA and vacancy distributions power-law of the type Ax^S was fitted (Figures 13 and 14). For SIA clusters the results seem to be rather similar regardless of temperature, however due to smaller sample size (20 compared to 30), the error is larger for 1900K. Additionally the fitting parameters are dominated by the distribution of the smaller clusters and the changes in large cluster size cause negligible change in the parameters. However looking at the graph itself, there seems to be an increase in larger clusters at 1900K deviating from the power-law unlike 800K which clearly follows the power-law.

For vacancy distributions, there is a much clearer difference; A is much larger at 1900K meaning more clusters however, S is larger for 800K which should mean larger clusters are relatively more common. However both distributions clearly differ from the power-law at higher cluster sizes. The power-law fit is accurate up to $\sim$100 vacancies for 800K, but only $\sim$50 for 1900K. For both distributions large clusters are clearly more common than a power-law distribution would suggest, especially at 1900K. This could be due to temperature fluctuations affecting smaller clusters more, causing the smaller defects to recrystallize, while larger defect clusters are affected less.

Type	N_{mean}	N_{min}	N_{max}
Vacancies 800K	640.9 ± 107.7	37	2066
Vacancies 1900K	526 ± 105.7	85	1906
SIAs 800K	93.9 ± 17.9	3	494
SIAs 1900K	139.4 ± 17.2	5	249
Sputtered atoms 800K	49.3 ± 12	0	291
Sputtered atoms 1900K	23 ± 10	0	185

Table 1: Average, minimum and maximum amount of created vacancies, SIAs or sputtered atoms

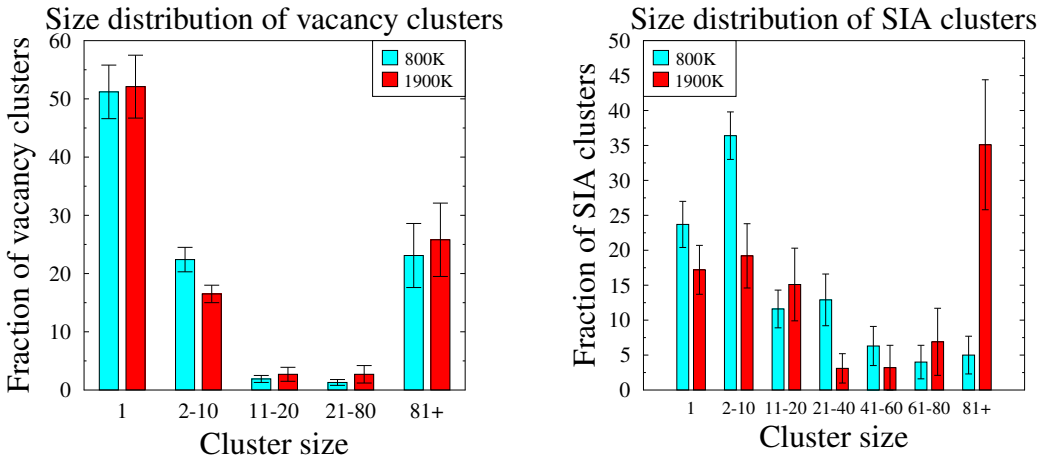

Figure 12: Size distribution of vacancy and SIA clusters.

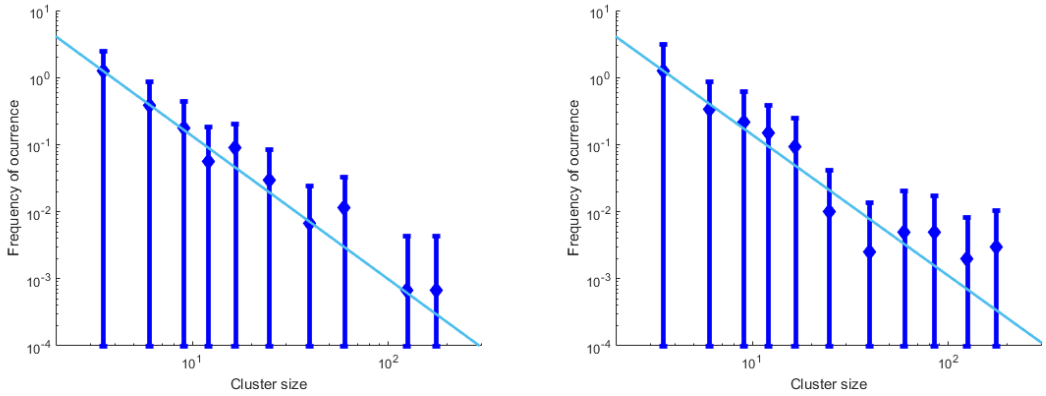

Figure 13: Power-law of type Ax^S fitted to SIA cluster size distribution. On the left we have distribution for 800K cascades while on the right we have the distribution for 1900K cascades. We get A=18.06 ± 3.55, S = -2.133 ± 0.145 at 800K and A = 17.52 ± 6.3, S = -2.1 ± 0.267 at 1900K. The error is the 95% confidence interval.

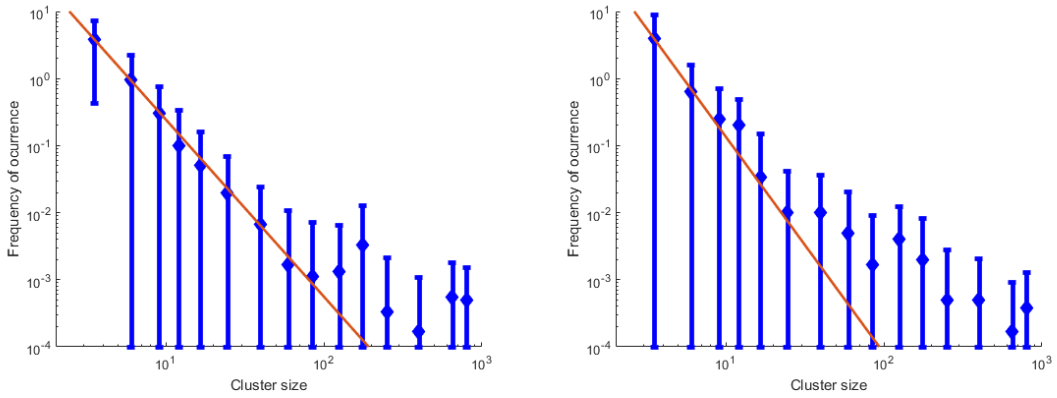

Figure 14: Power-law of type Ax^S fitted to vacancy cluster size distribution. On the left we have distribution for 800K cascades while on the right we have the distribution for 1900K cascades. We get A=105.6 ± 8.8, S = -2.639 ± 0.064 at 800K and A = 223.5 ± 62.5 , S = -3.223 ± 0.219 at 1900K. The error is the 95% confidence interval.

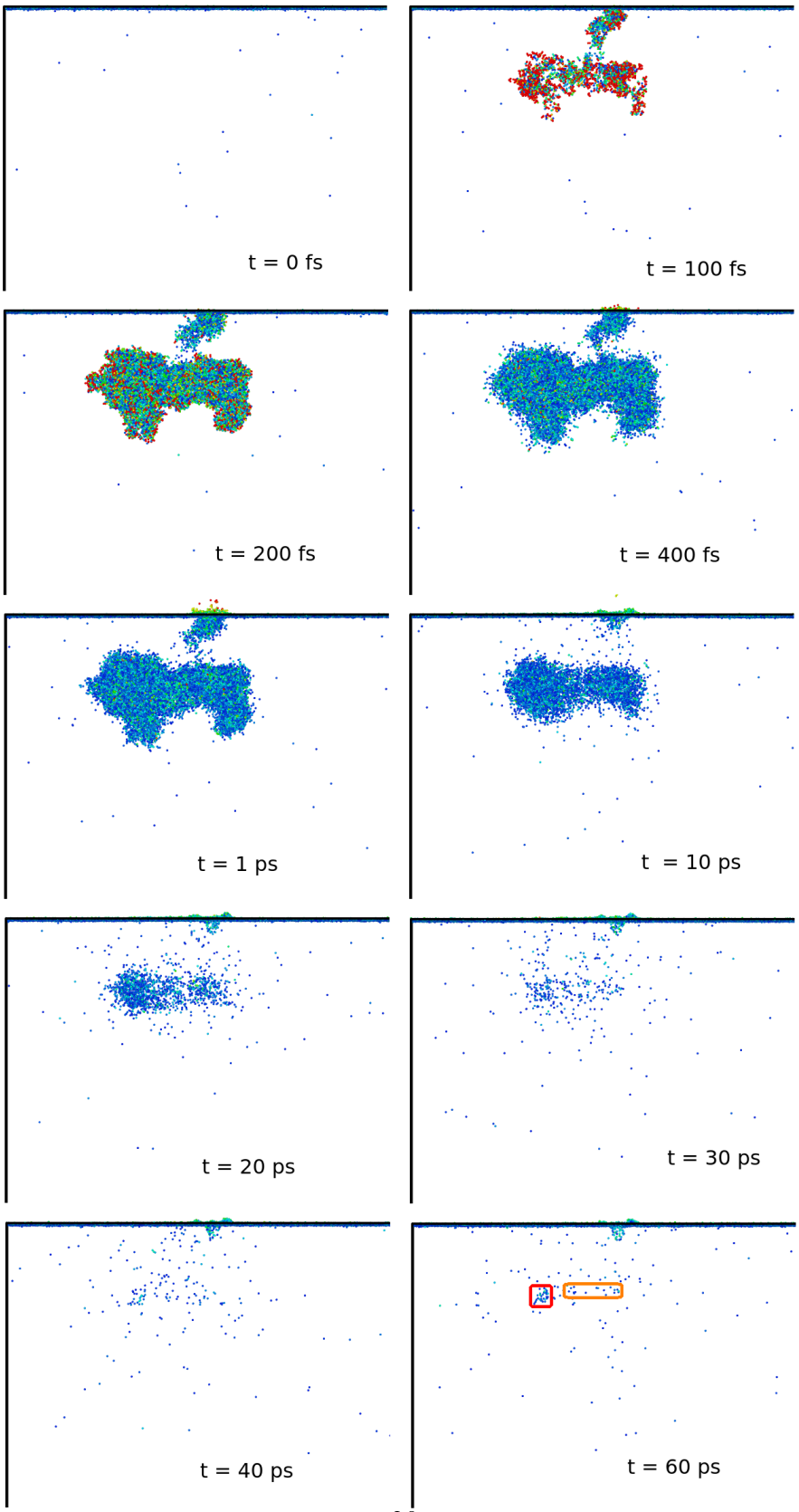

Figure 15: Cascade over time. Colors indicate potential energy (red = high, blue=low). Circled in the last frame are two spots where defect clusters were seen to form (SIA loop in orange, vacancy cluster in red).

6 Effect of plasma impurities on tungsten surfaces

Hot plasma inside the fusion reactor is prone to instabilities. The plasma instabilities can create energy surges which damage the reactor surfaces. One way to prevent instability is to cool down the plasma. However, increasing the stability reduces the efficiency of the reaction.

Cooling down the plasma can be achieved by injecting a small amount of noble gases into the plasma [30]. These gases ionize due to the extreme heat, cooling down the plasma therefore preventing possible instabilities. Noble gases are chosen due to their chemical inertness.

The noble gas ions do not contribute to the fusion reaction and are thus considered as impurities and will end up being removed from the plasma by the divertor at the bottom of the reactor.

The main material for the plasma facing part of the divertor is tungsten. This means that the divertor's tungsten surface, in addition to heat and bombardment by plasma components, must also handle noble gas irradiation. At energies below 300 eV, tungsten sputtering due to deuterium ions is essentially 0. However this may not be the case if there are noble gas impurities. Thus it is important to find out the effect of noble gas impurities on the sputtering of tungsten surfaces. [31]

For this reason I have simulated the co-bombardment of a tungsten surface with deuterium, neon and argon. Due to its abundance in the plasma, most irradiation the divertor experiences consists of deuterium. The noble gas impurities are much heavier and larger than deuterium. This may have a large effect on the damage caused to the surface and on the deuterium retention of the surface. This means that studying the effect of these additional species on the sputtering behavior and surface morphology is of particular interest.

6.1 Methods

Simulations were performed using the molecular dynamics code PARCAS [27] using Juslin et al potential [32] for the W atoms, while the interaction models between the gases (D, Ne, Ar) themselves and between the gases and the tungsten atoms were Ziegler-Biersack-Littmark (ZBL) pair potentials [18]. Simulations were started by creating a body center cubic (BCC) lattice with a 110-surface consisting of pure tungsten with the size of roughly 30x30x60 Å. The lattice was periodic in x and y directions with no periodicity in z. The two bottomost layers had a fixed position, while the two layers above those were connected to a Berendsen thermostat [33] keeping a constant temperature in order to simulate a surface connected to bulk material. This lattice was then relaxed for 100ps at both 500K and 800K to create the initial lattices for irradiation.

After relaxation, cumulative irradiation of the lattice with deuterium and noble gas impurities was simulated. For both temperatures, five different irradiation energies (10, 30, 50, 80, 100 eV) were tested along with different concentrations (0, 5, 10, 20%) and different impurity types (neon or argon). Additionally for pure deuterium cases, three higher energy cases of 150, 200 and 300 eV were tested.

At the start the input lattice was randomly shifted by up to half of the box size in x and y-directions in order to ensure even irradiation of the surface. Irradiation was simulated by creating an ion of the specified energy 5 Å above the surface at the center of the simulation cell with velocity straight towards the surface. Depending on the concentration 5,10 or 20% of the ions were randomly chosen using the Mersenne Twister algorithm [34] to be a noble gas impurity instead of deuterium. The system was then simulated for 7 ps, after which the end result of the simulation was saved and used as a starting point for the next irradiation event. 7 ps was determined to be sufficiently long for the system to relax despite leading to a very high flux. However reaching practical fluxes in MD simulations requires impractical amounts of computing power. This process was repeated 2000 times to achieve 2000 cumulative bombardments for every combination of energy, impurity and concentration.

After every irradiation event, the sputtered atoms were analysed and a cluster analysis was performed on sputtered atoms to find out if sputtered species were molecules or single atoms. Special attention was paid to cases with W sputtering and especially sputtering of WD_n molecules.

6.2 Results

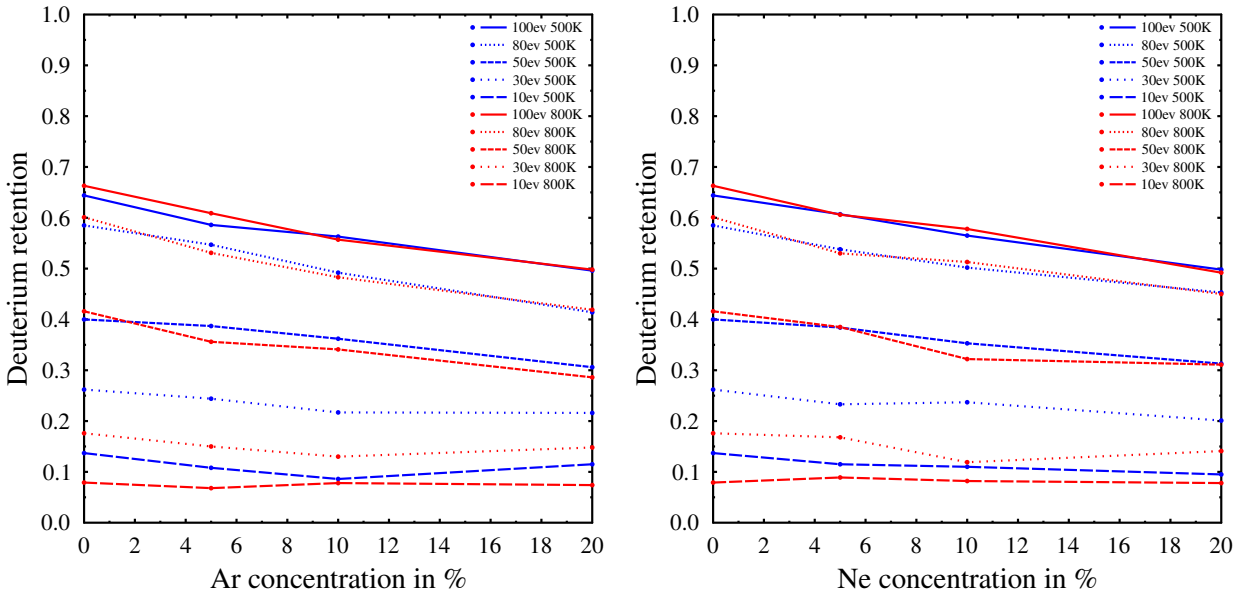

Figure 16: Deuterium retention. Calculated by dividing the amount of deuterium in the system at the end compared to all deuterium irradiation events for the system.

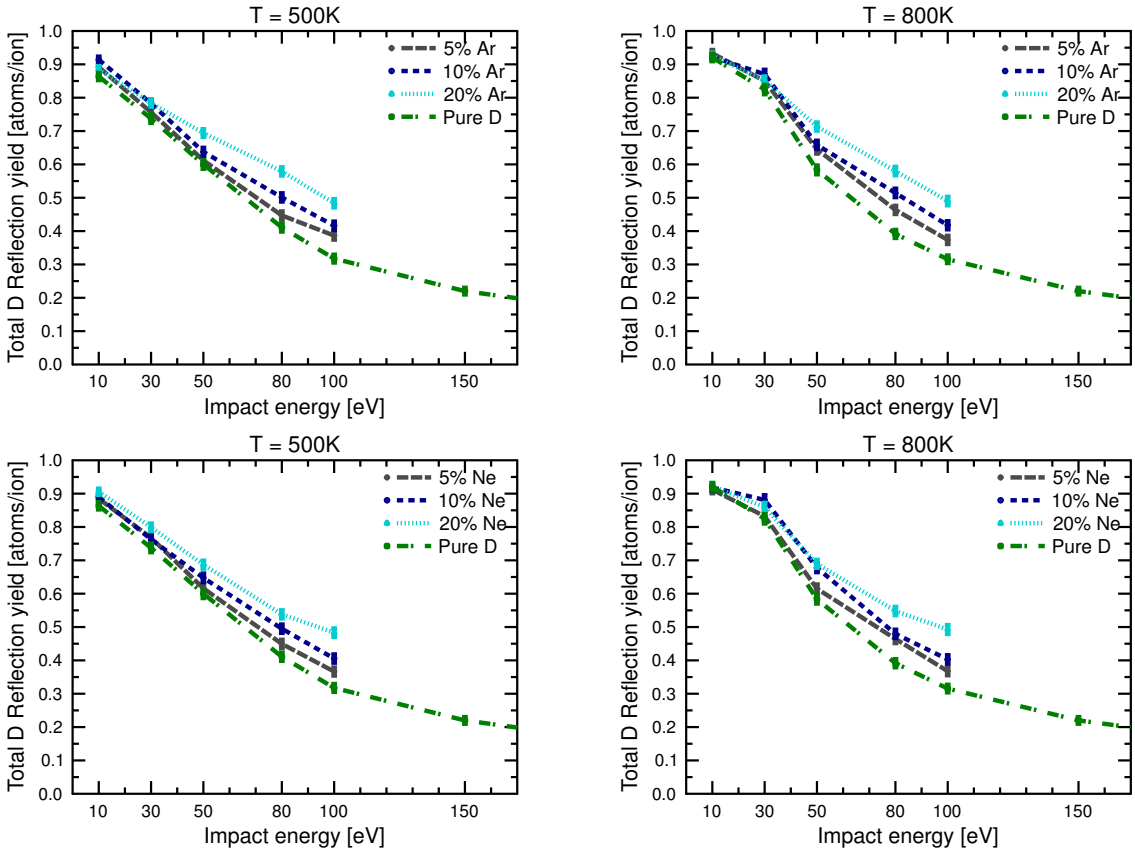

Figure 17: Deuterium reflection yield

Deuterium reflection (Figure 17) clearly decreases with increasing ion energy. This is simply due to increased kinetic energy making it easier to penetrate into the material instead of reflecting from the surface. The effect of temperature seems minimal at higher energies but there is a clear difference at lower energies. Additionally the concentration seems to increase the deuterium reflection at higher energies with very little impact at lower ones. This could be due to the increased surface damage caused by impurities at higher energies leading to more reflection.

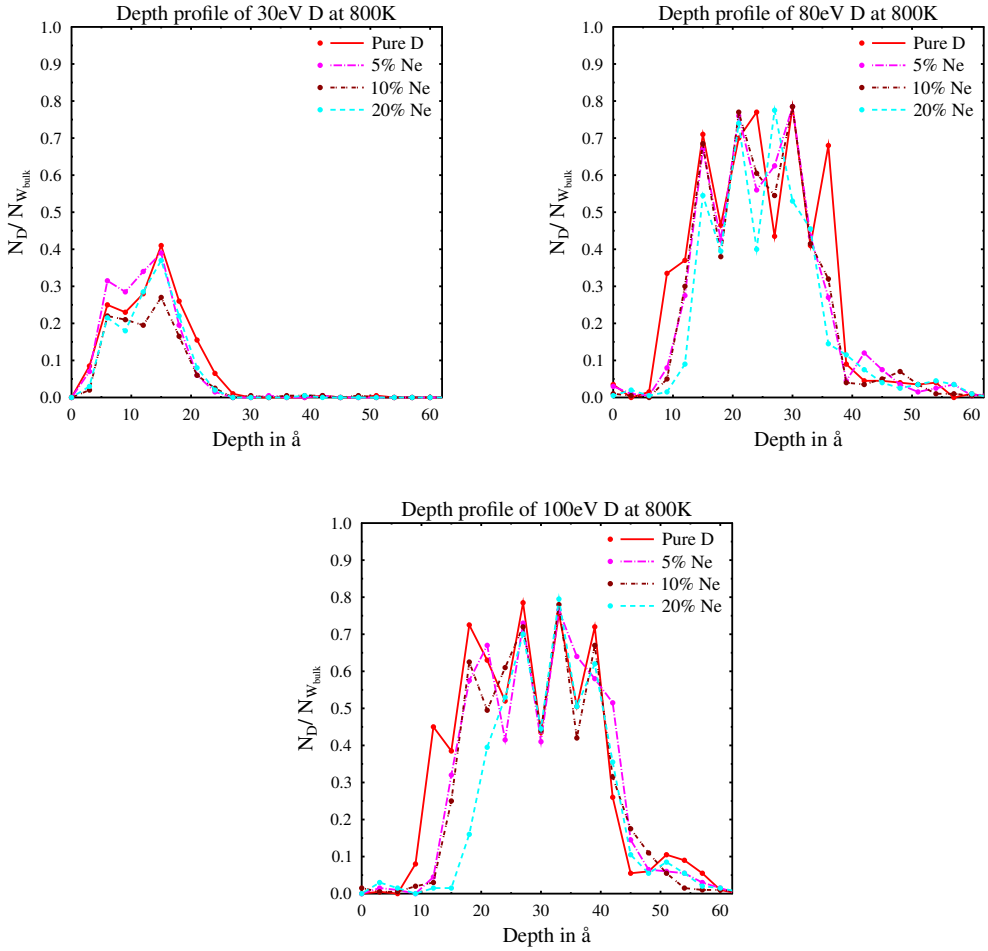

Figure 18: Depth profile of absorbed Deuterium.

From Figure 18 we can see that the D penetrates deeper into the surface at higher energies and is spread over a wider area. There is also more deuterium which is consistent with D reflection decreasing with ion energy. Concentration of noble gas impurities seems to have minimal effect on the D depth profile except at higher energies where increased impurity concentration seems to cause slight depletion of D at the surface. Concentration seems to increase the D reflection yield, so perhaps the damage caused to the surface prevents deuterium build up near it or the reduced deuterium retention does not allow for the D rich region to expand as

much towards the surface. Transition from crystalline to amorphous can also be seen in Figure 19, where the build-up of D ions has clearly turned the tungsten structure from crystalline to fully or partly amorphous.

Deuterium ions seemed to prefer sites close to other deuterium ions leading to build up in specific spots of the lattice. At higher energies when the build-up of D ions happened beneath the surface rather than on it, the D ions caused the lattice to slightly swell, rising the surface by up to 3Å. However there was no rupturing of the surface.

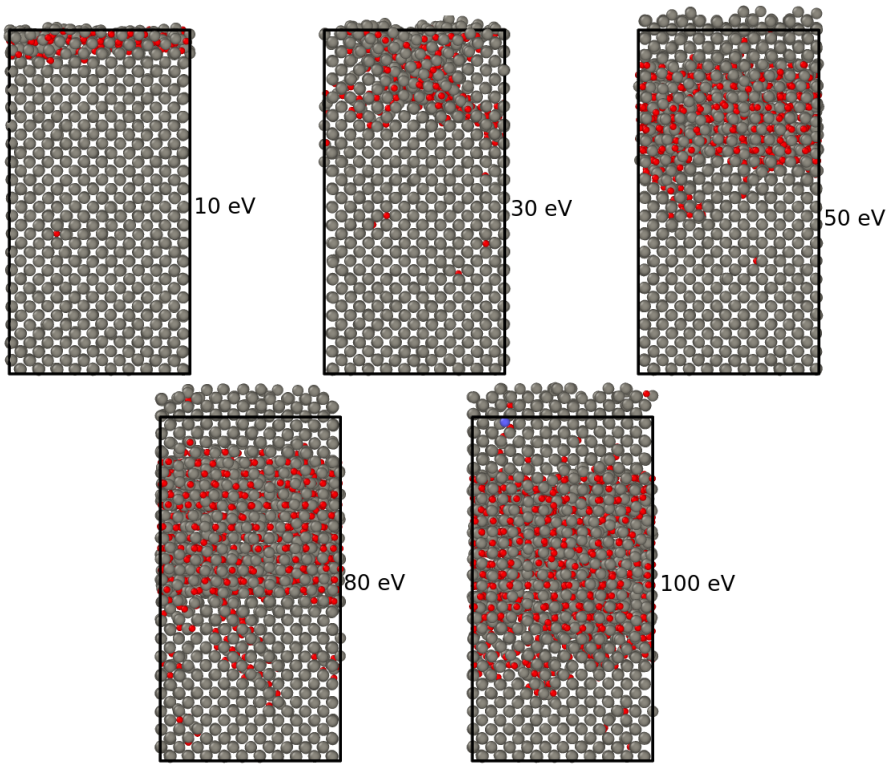

Figure 19: Tungsten lattice after bombardment by deuterium and neon (10% Ne concentration) of different energies at 800K. Gray atoms are tungsten and red atoms are deuterium. The blue atom in the 100 eV case is neon. Black lines represent the original lattice.

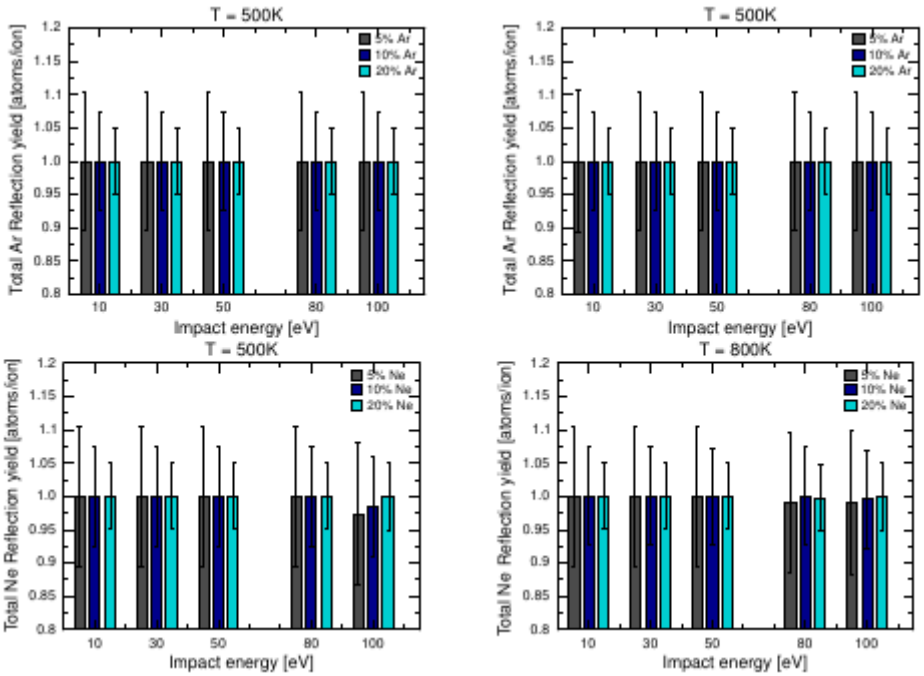

Figure 20: Reflection of noble gases. Error bars represent the standard error and are merely an indicator of accuracy rather than range of probable values (since yields of more than 1.0 are impossible in this scenario)

Reflection of noble gas impurities (Figure 20) was 100% for all Ar cases while some Ne cases had reflection of slightly less than 100% but no more than 97%. Ar ions seemed to be unable to penetrate into the surface while some Ne ions penetrated just deep enough where they could act as substitutional defects in the tungsten lattice. However these Ne impurities were not stable and would try to move to other nearby vacancies if possible and once near the surface they would escape the lattice completely.

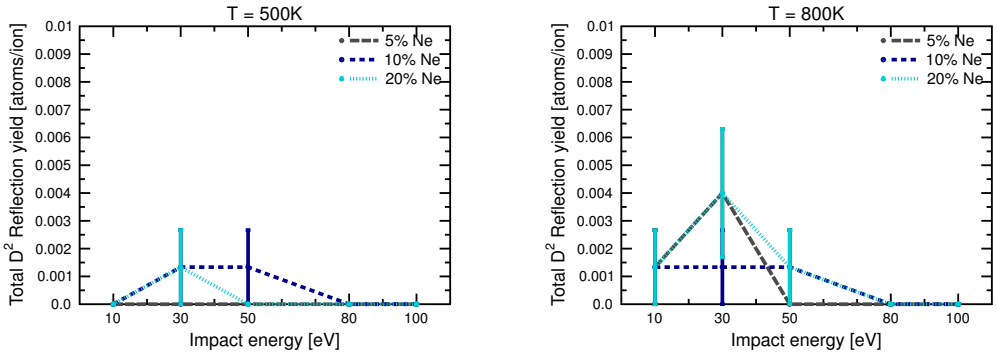

Figure 21: Sputtering of D^2 molecules.

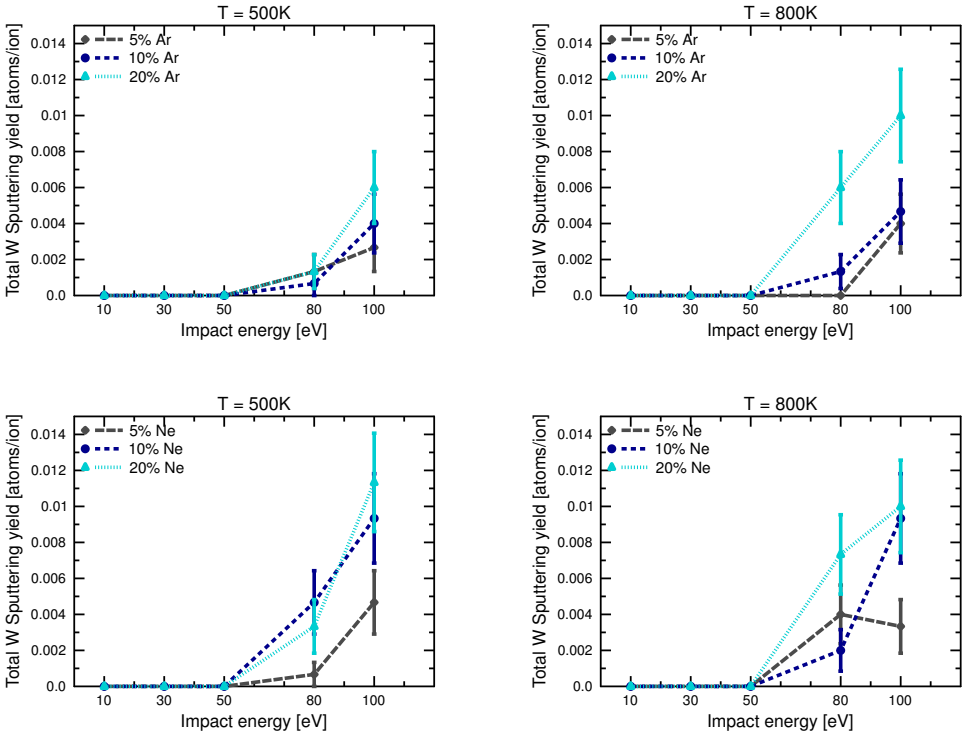

Figure 22: Tungsten sputtering yield

D_2 sputtering (Figure 21) was rare but certainly possible for energies 50 eV and lower. The lack of molecular deuterium sputtering for higher energies is probably explained simply by the lack of D atoms at the surface at higher energies compared to lower ones which increases the chance of both sputtering and D atoms forming bonds. At least for neon cases and pure deuterium cases, the sputtering yield of D_2

molecules seemed to increase with the temperature, though there were not enough cases to determine this with confidence

The tungsten sputtering (Figure 22) did not happen at lower energies ($\leq$50 eV). There was also no W sputtering for pure D cases even at 300 eV, which seems to be in agreement with experimental results. [31] However, at 80 eV and above, the addition of noble gas impurities made W sputtering possible. W sputtering increases with both energy and impurity concentration. Since there was no sputtering at lower energies, sputtering is not swift chemical sputtering in nature, but rather physical sputtering. [35] There seemed to be no statistically significant T dependence.

In addition to W sputtering, the surface was otherwise damaged during the bombardment. At energies of 50 eV and below, the deuterium ions gathered at the surface, changing the structure from crystalline to non-crystalline due to the high concentration of deuterium. At higher energies, the surface itself remained almost completely intact during pure D bombardment, with damage happening deeper in the lattice. However, when noble gas impurities were introduced, at higher energies the surface suffered notable damage. It remained crystalline but became much rougher. The amount of damage the surface received increased with both ion energy and impurity concentration.

There were 6 cases of WD molecular sputtering, which is not enough for statistical analysis, however the existence of multiple such events is still an important result. Five such cases happened when 100 eV Ne impurity collided with the surface and one with a 80 eV Ar impurity. Both 500K and 800K had cases of WD sputtering. WD sputtering also happened early on (300 irradiations in) and late (1900 irradiations in). The mechanism of WD sputtering seemed to be that a D atom was bound to nearby W atoms. Then the impurity ion knocks the W atom away from the surface and during this the D atom that was bound sticks with the W atom causing a WD molecule to be sputtered. This, combined with the high energies of the impurities, means that the WD sputtering mechanism is likely physical in nature. An example event can be seen in Figure 23.

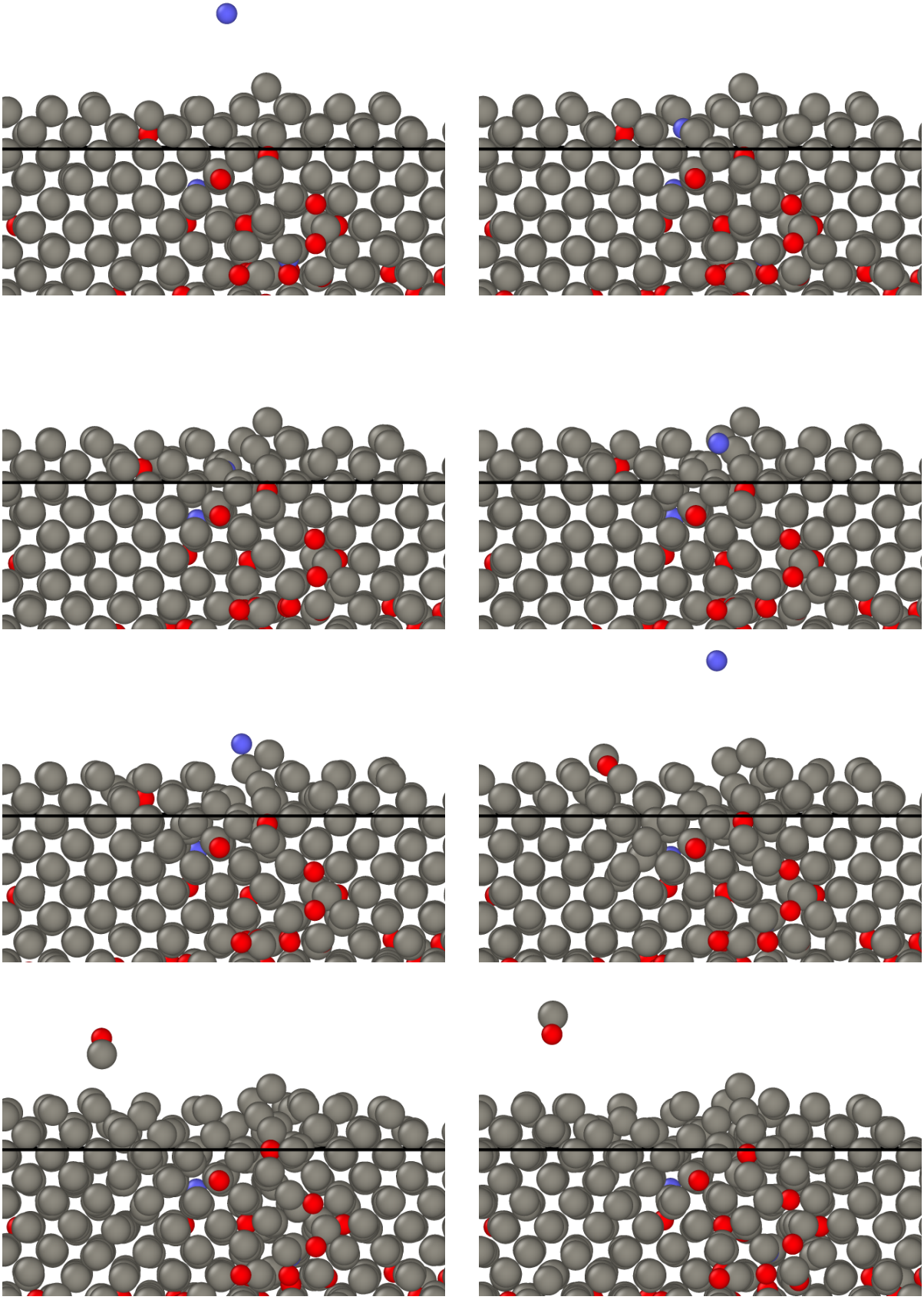

Figure 23: Sputtering event of WD molecule. Ne ion colored blue, D red and W gray.

7 Summary

In high energy cascades, heat spikes in tungsten cause the formation of defect clusters. In my simulations, this resulted mostly in the formation of SIA loops of the types <100> and $\frac{1}{2}$ <111>. Vacancy loops of the type <100> were also seen, however the lack of $\frac{1}{2}$ <111> vacancy loops, which are found in experiments [1] is puzzling. Additionally the damage clusters included craters and spherical voids. A large temperature difference of over 1000K did not have a large impact on damage formation when it came to the amount of defects or their type distribution. However, there was a noticable difference in the size distribution of the defect clusters. For both vacancy and SIA clusters, an increased temperature caused the distribution to be more skewed towards larger clusters. Thus we can conclude from the simulations that the increase in the temperature results in roughly the same amount of defects. However the resulting defects will be larger on average.

The inclusion of noble gas impurities in low energy co-bombardment of a tungsten surface with deuterium was simulated. Bombardment with pure D resulted in no sputtering of tungsten, even at higher energies (300 eV). However the introduction of either neon or argon to the bombardment resulted in at least some sputtering at 80 eV and 100 eV. This means that the impurities cause a clear difference in the damage the surface receives. An increase in the sputtering yield when the noble gas concentration was increased was also noted.

An increase in the purity concentration also caused a decrease in deuterium retention in the material. This is most likely due to increased damage done to the surface causing the now uneven surface to reflect more incoming deuterium. This effect was more pronounced at higher impact energies, where the surface receives more damage. At higher impact energies the deuterium retention increased due to the ions being able to penetrate deeper into the material instead of being reflected back. This build up of deuterium caused the amorphization of the material. An increase in the impurity concentration tended to decrease this retention due to increased reflection yield.

Additionally, the effect of a temperature difference was investigated for the co-bombardment. A higher temperature caused an increase in deuterium reflection at smaller energies, however, the effect was not noticable at higher energies. There was no statistically significant difference in tungsten sputtering due to the rarity of these events. Attention was also paid to the sputtering of molecules. At low energies D_2 sputtering was noted to happen when noble gas impurities were present. This was not noted at higher energies because there was no surface build up of D that was noted at lower impact energies, which made formation of D_2 molecules unlikely. Interestingly, sputtering of WD molecules happened for both neon and argon bombardment. This is significant because that molecule species isn't usually taken into account, while it perhaps should be.

8 Bibliography

References

[1] X. Yi, M.L. Jenkins, M. Briceno, S.G. Roberts, Z. Zhou, and M.A. Kirk. In situ study of self-ion irradiation damage in W and W-5Re at 500 C. *Philosophical Magazine*, 93(14):1715–1738, 2013.

[2] ITER Physics Basis Editors, ITER Physics Expert Group Chairs, Co-Chairs, ITER Joint Central Team, and Physics Integration Unit. Iter physics basis, 1999.

[3] Fuelling the fusion reaction. `https://www.iter.org/sci/fusionfuels` (Accessed 5.11.2018).

[4] H. Zerriffi, H. Scoville Jr., and P. Fellow. Tritium: The environmental, health, budgetary, and strategic effects of the department of energy's decision to produce tritium. *Report by US Institute for Energy and Environmental Research*, 1996.

[5] Tritium breeding. https://www.iter.org/mach/tritiumbreeding (Accessed 5.11.2018).

[6] Reaching 150,000,000c. https://www.iter.org/sci/plasmaheating (Accessed 5.11.2018).

[7] J. Wesson. *Tokamaks, 3rd ed.* Oxford University Press, 2004.

[8] Schematic of a tokamak reactor. https://www.power-technology.com/wp-content/uploads/sites/7/2017/10/Tokamak.jpg (Accessed 5.11.2018).

[9] D. Post, J. Abdallah, R. E. H. Clark, and N. Putvinskaya. Calculations of energy losses due to atomic processes in tokamaks with applications to the international thermonuclear experimental reactor divertor. *Physics of Plasmas*, 2(6):2328–2336, 1995.

[10] Plasma confinement. https://www.iter.org/sci/plasmaconfinement (Accessed 5.11.2018).

[11] H Bolt, V Barabash, W Krauss, J Linke, R Neu, S Suzuki, N Yoshida, and ASDEX Upgrade Team. Materials for the plasma-facing components of fusion reactors. *Journal of Nuclear Materials*, 329-333:66 – 73, 2004.

[12] M J Rubel, V Bailescu, J P Coad, T Hirai, J Likonen, J Linke, C P Lungu, G F Matthews, L Pedrick, V Riccardo, P Sundelin, E Villedieu, and JET-EFDA Contributors. Beryllium plasma-facing components for the iter-like wall project at jet. *Journal of Physics: Conference Series*, 100(6):062028, 2008.

[13] Divertor. https://www.iter.org/mach/Divertor (Accessed 5.11.2018).

[14] M. Rieth, S.L. Dudarev, S.M. Gonzalez de Vicente, J. Aktaa, T. Ahlgren, S. Antusch, D.E.J. Armstrong, M. Balden, N. Baluc, M.-F. Barthe, W.W. Basuki, M. Battabyal, C.S. Becquart, D. Blagoeva, H. Boldyryeva, J. Brinkmann, M. Celino, L. Ciupinski, J.B. Correia, A. De Backer, C. Domain, E. Gaganidze, C. Garcia-Rosales, J. Gibson, M.R. Gilbert, S. Giusep-

poni, B. Gludovatz, H. Greuner, K. Heinola, T. Höschen, A. Hoffmann, N. Holstein, F. Koch, W. Krauss, H. Li, S. Lindig, J. Linke, Ch. Linsmeier, P. Lopez-Ruiz, H. Maier, J. Matejicek, T.P. Mishra, M. Muhammed, A. Munoz, M. Muzyk, K. Nordlund, D. Nguyen-Manh, J. Opschoor, N. Ordas, T. Palacios, G. Pintsuk, R. Pippan, J. Reiser, J. Riesch, S.G. Roberts, L. Romaner, M. Rosiński, M. Sanchez, W. Schulmeyer, H. Traxler, A. Urena, J.G. van der Laan, L. Veleva, S. Wahlberg, M. Walter, T. Weber, T. Weitkamp, S. Wurster, M.A. Yar, J.H. You, and A. Zivelonghi. A brief summary of the progress on the efda tungsten materials program. *Journal of Nuclear Materials*, 442, 2013.

[15] Picture of the iter divertor. `http://fusionforenergy.europa.eu` (Accessed 5.11.2018).

[16] G. Was. *Fundamentals of Radiation in Materials Science: Metals and Alloys.* Springer London, Limited, 2007.

[17] J. F. Siegler. Srim-2013.00 software package, available online at. `http://www.srim.org`, 2013.

[18] Ziegler J F, Biersack J P, and Littmark U. The stopping and range of ions in matter (newyork: Pergamon), 1985.

[19] M. P. Allen and D. J. Tildesley. *Computer Simulation of Liquids (Oxford Science Publications).* Oxford science publications. Oxford University Press, reprint edition, June 1989.

[20] M. Born and R. Oppenheimer. Zur quantentheorie der molekeln. *Annalen der Physik*, 389(20):457–484, 1927.

[21] On the determination of molecular fields. —ii. from the equation of state of a gas. *Proceedings of the Royal Society of London A: Mathematical, Physical and Engineering Sciences*, 106(738):463–477, 1924.

[22] S. Daw Murray and M. I. Baskes. Embedded-atom method: Derivation and application to impurities, surfaces, and other defects in metals. *Physical Re-*

view B, 29(12), 1984.

[23] K. Nordlund. Molecular dynamics simulation of ion ranges in the 1 – 100kev energy range. *Comput. Mater. Sci. 3*, 3(4):448, 1995.

[24] H. Bethe and J. Ashkin. *Experimental Nuclear Physics*. J. Wiley, 1953.

[25] P. Sigmund. *Stopping of heavy ions: A theoretical approach*, volume 204. Springer Tracts in Modern Physics, 2004.

[26] A. Hinchliffe. *Molecular modelling for beginners*. Wiley, 2008.

[27] K. Nordlund. Parcas computer code, 2006.

[28] N. W. Ashcroft and N. D. Mermin. *Solid State Physics*. Saunders, 1976.

[29] Alexander Stukowski. Visualization and analysis of atomistic simulation data with OVITO–the Open Visualization Tool. *Modelling and Simulation in Materials Science and Engineering*, 18(1):015012, 2010.

[30] Parker R, Janeschitz G, Pacher H D, Post D, Chiocchio S, Federici G, and Ladd P. Plasma–wall interactions in iter. *J. Nucl. Mater.*, 241-243:1–26, 1997.

[31] K. Sugiyama, K. Schmid, and W. Jacob. Sputtering of iron, chromium and tungsten by energetic deuterium ion bombardment. *Nuclear Materials and Energy*, 8:1 – 7, 2016.

[32] Erhart P Juslin N, Äskelin P, Nord J, Henriksson K O E, Nordlund K, Salonen E, and Albe K. Analytical interatomic potential for modelling non-equilibrium processes in the w–c–h system j, 2005.

[33] H. J. C. Berendsen, J. P. M. Postma, W. F. van Gunsteren, A. DiNola, and J. R. Haak. Molecular dynamics with coupling to an external bath. *The Journal of Chemical Physics*, 81(8):3684–3690, 1984.

[34] Makoto Matsumoto and Takuji Nishimura. Mersenne twister: A 623-dimensionally equidistributed uniform pseudo-random number generator. *ACM Trans. Model. Comput. Simul.*, 8(1):3–30, January 1998.

[35] K. Nordlund, E. Salonen, and A. Krasheninnikov et al. Swift chemical sputtering of covalently bonded materials. *Pure and Applied Chemistry*, 78:1203–1211, 2009.